

Synthesis and optical properties of monodispersed Ni²⁺-doped ZnS nanoparticles

G. Murugadoss · M. Rajesh Kumar

Received: 17 September 2012 / Accepted: 12 October 2012 / Published online: 30 October 2012
© The Author(s) 2012. This article is published with open access at Springerlink.com

Abstract Nickel-doped zinc sulfide nanoparticles were successfully synthesized in air atmosphere through chemical precipitation method using surfactants in aqueous medium. The product was characterized by different techniques such as X-ray diffraction (XRD), transmission electron microscopy (TEM), fourier transform infrared spectrometer (FT-IR), UV–visible absorption and photoluminescence (PL). Crystal structure, size and morphology of the ZnS:Ni²⁺ nanoparticles were investigated by XRD and TEM. In the PL emission, a couple of new peaks were observed instead of a single peak by changing the precursor solution. In addition, an enhanced PL emission was observed using surfactants. Phase changes were also observed at different temperatures.

Keywords Nanostructures · Semiconductors · Chemical synthesis · Oxidation

Introduction

There has been much interest recently in synthesizing nanometer-sized semiconductor particles because such particles exhibit size-dependent optical and electrical properties. The nanocrystalline materials are good candidates for application in optoelectronic devices due to their

reduced size, enabling a reduction in the size of the electronic circuit. Moreover, it is also possible to tune their properties to suit a specific application by merely changing their size (Sampra and Sarma 2004). When compared to their bulk counterparts, semiconductors in the nanoparticle range also exhibit different behavior. Decreasing the particle size gives rise to quantum confinement effect (Brus 1986), wherein an increase in the energy gap as well as splitting of the conduction and valence bands into discrete energy levels becomes evident. These particles are expected to have higher quantum efficiencies in applications such as light emitters.

Doping with optically active luminescent materials manipulates the band structure of the nanoparticles and show intense emissions in a wide range of wavelength depending on the impurity type, concentration and crystal dimensions, and also play key roles in luminescence efficiency and the positions of emission bands, thus influencing their practical applications. The doped luminescent nanoparticles are of strong interest for possible use in optoelectronics such as LEDs and lasers or as novel phosphors because of their interesting magnetic (Kennedy et al. 1995; Counio et al. 1996; Igarashi et al. 1997; Feltin et al. 1999) and electro-optical properties (Murugadoss et al. 2010; Pohl and Gumlich 1989; Devisschere et al. 1995; Yu et al. 1998). Recently, the doped nanomaterials have been largely studied due to their widespread applications in various devices such as sensors, solar cells, lasers, photocatalysts, photodetectors, IR detectors, optical communication, color television, flat panel display, phosphors, light emitting diodes, etc. (Ong and Chang 2001; Fang et al. 2009; Kar and Biswas 2008; Becker and Bard 1983; Klimov et al. 2007; Wang et al. 2005; Green and Hersam 2008; Toyama et al. 2009; Brus 1991; Hoffman et al. 1992).

G. Murugadoss (✉)
Centre for Nanoscience and Technology, Anna University,
Chennai 600 025, Tamilnadu, India
e-mail: murugadoss_g@yahoo.com

M. Rajesh Kumar
Department of Physics, Annamalai University,
Annamalai Nagar 608 002, Tamilnadu, India

Among the various semiconductor compounds, the nanocrystals belonging to II–VI groups were the most studied since they exhibit interesting size-tunable optical properties due to the strong quantum confinement effect (Alivisatos 1996). Especially, zinc sulfide is an important II–VI group semiconductor compound with direct wide band gap energy of 3.67 eV at room temperature. Therefore, in this work the ZnS has been chosen as a host material to synthesize doping nanoparticles for enhanced optical properties. In doped ZnS nanocrystals, impure ion occupies the Zn lattice site and behaves as a trap site for electron and holes. The electrons are excited from the ZnS valence band to conduction band by absorbing the energy equal or greater than their band gap energy. Subsequent relaxation of these photo-excited electrons to some surface states or levels is followed by radiative decay enabling the luminescence in visible region.

Several techniques have been used to synthesize doped ZnS nanoparticles such as sol–gel, chemical precipitation, solid state reaction, auto-combustion, etc. In this paper, the ZnS nanoparticles with varying initial doping concentrations (0.5–5 %) of Ni^{2+} were synthesized through a chemical precipitation method, as it is simple, inexpensive and more productive. The luminescence properties of the ZnS: Ni^{2+} nanoparticles were investigated by photoluminescence (PL) spectroscopy. The optical study was adopted to determine the actual doping concentrations. To promote a confined and stable growth of ZnS: Ni^{2+} nanoparticles, the capping molecules PMMA, PEG, PVP and CTAB were used in the reaction process. It is indicated that the addition of capping molecule could greatly influence the PL emission and size confinement of ZnS: Ni^{2+} nanostructures. The objective of the present study is to synthesize luminescent ZnS doped with transition metal Ni^{2+} and create bio-organic interface with bio-compatible inorganic/organic material for possible use as nanoscale fluorescent probes for potential pharmaceutical, biological and medical applications such as targeted drug delivery and labeling of biological cells.

Experimental

Materials

To synthesize ZnS and ZnS: Ni^{2+} , the following materials were used. All the glassware used in this experimental work were acid washed. The chemicals used were analytical reagent grade without further purification. Ultrapure water was used for all dilution and sample preparation. Zinc acetate dehydrate [$\text{Zn}(\text{CH}_3\text{COO})_2 \cdot 2\text{H}_2\text{O}$], nickel acetate [$\text{Ni}(\text{CH}_3\text{COO})_2 \cdot 4\text{H}_2\text{O}$] and sodium sulfide ($\text{Na}_2\text{S} \cdot x\text{H}_2\text{O}$) obtained from Nice Chemical company were

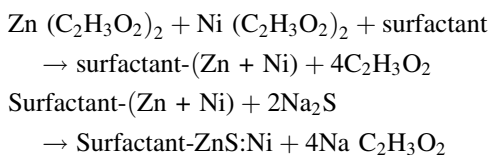
used as precursors. Poly methyl methacrylate (PMMA-1,20,000) and polyvinylpyrrolidone (PVP-40,000) were obtained from Aldrich and Otto Chemika, respectively. Polyethylene glycol (PEG-6,000–7,000) and cetyltrimethylammonium bromide (CTAB-364.46) were obtained from S. D fine Chem. Ltd and Spectrochem. Pvt. Ltd, respectively. All the chemicals are above 98 % purity.

Synthesis of ZnS: Ni^{2+} nanoparticles

The ZnS nanoparticles doped with different Ni^{2+} concentrations were synthesized in de-ionized water at air atmosphere. In a typical experiment, 5.48 g (0.5 M) of $\text{Zn}(\text{CH}_3\text{COO})_2 \cdot 2\text{H}_2\text{O}$ in 50 ml aqueous and $\text{Ni}(\text{CH}_3\text{COO})_2 \cdot 4\text{H}_2\text{O}$ in 25 ml aqueous with different concentrations (0.5, 1.0, 1.5, 2, 3, 4 and 5 %) were mixed drop by drop. The concentration of Ni^{2+} was adjusted by controlling the quantity of nickel acetate in the above mixture. The mixture was stirred magnetically at 80 °C until a homogeneous solution was obtained. Then, 2.75 g (0.5 M) of 50 ml Na_2S was added drop by drop to the above mixture. After the Na_2S injection a white, voluminous precipitate appears. It slowly dissolves under the formation of ZnS: Ni^{2+} nanoparticles during incubation under stirring for 30 min at 80 °C. The obtained dispersions are transparent and were purified by dialysis against de-ionized water and ethanol several times to remove impurities. The products were dried in hot air oven at 80 °C for 2 h. The undoped ZnS nanoparticle was synthesized following the same procedure in the absence of the doping material.

Synthesis of surfactants capped ZnS: Ni^{2+} nanoparticles

To synthesize surfactants capped ZnS: Ni^{2+} nanoparticles, poly methyl methacrylate (PMMA), polyvinyl pyrrolidone (PVP), polyethylene glycol (PEG) and cetyltrimethylammonium bromide (CTAB) were used as stabilizing agents. The concentration of surfactants is limited i.e., 0.5 g. The surfactants were prepared individually in 50 ml of de-ionized water using magnetic stirrer to completely dissolve. Following the same synthesis steps, newly prepared surfactants were added into zinc acetate solution before adding nickel acetate with continuous stirring. Then, following the other steps continuously (in “[Synthesis of ZnS: \$\text{Ni}^{2+}\$ nanoparticles](#)”), surfactants capped ZnS: Ni^{2+} nanoparticles were synthesized. Thus obtained nanoparticles were washed several times by acetone and alcohol. Washing was carried out to remove the byproducts and the excessive surfactants that were bound with the nanoparticles. After washing, the nanoparticles were dried at 80 °C for 2 h. The surfactant capped ZnS: Ni^{2+} nanoparticles were synthesized by following simple reaction in aqueous solution:



Characterization

The X-ray diffraction (XRD) patterns of the powdered samples were recorded using X'PERT PRO diffractometer with a Cu-K α radiation ($\lambda = 1.5406 \text{ \AA}$). The crystallite size was estimated using the Scherrer equation of the major XRD peak. The morphology and size of the nanoparticles were analyzed through TEM (PHILIPS-CM200; 20–200 kV) microscopy. In addition, the particle size distribution of the capped particles was obtained by particles size analyzer (Nanotracs Specifications Model: Nanotracs NPA 150). The FT-IR spectra were obtained on an AVATOR 360 spectrometer using KBr pellet technique. The optical absorption spectra of all the samples in de-ionized water were recorded using UV-1650PC SHIMADZU spectrometer. Fluorescence measurements were performed on a RF-5301PC spectrophotometer. Emission (350–600 nm) spectra were recorded under the different excitation wavelengths at room temperature.

Results and discussion

Crystal structure and morphology

X-ray diffraction pattern gives information about crystal-line structure and grain size. Figure 1 shows the X-ray diffraction pattern of the ZnS, different concentrations (0.5, 1.0, 3 and 5 %) of Ni $^{2+}$ -doped ZnS and surfactant (PMMA, PEG, PVP and CTAB) capped ZnS:Ni $^{2+}$ (1 %) nanoparticles. The XRD pattern of all samples have three main diffraction features corresponding to (1 1 1), (2 2 0) and (3 1 1) planes. The broadening of the diffraction peaks indicates the nanosize of the synthesized particles. With increasing concentration of the nickel doping in the samples, the spectra remain the same, indicating that the cubic structure is not tailored by the addition of Ni into the ZnS matrix at least up to the detection level of XRD. Moreover, it indicates that the Ni ion successfully occupied ZnS lattice site and there were no secondary phases or precipitates in the sample. The similar crystallite size, stable cubic structure and absence of impurity phases with increasing concentration of Ni $^{2+}$ doping for all the samples could be attributed to the similarity in size of Zn and Ni ions. Ionic radius of Ni $^{2+}$ is 0.69 Å and Zn $^{2+}$ is 0.74 Å (Huang et al. 2009). In addition, the diffraction peaks of ZnS:Ni $^{2+}$ have no change by adding surfactants. This indicates that the surfactant molecules do not enter into the nanoparticles.

They only get adsorbed on the surface of the particles. However, the full width at half maximum (FWHM) of the diffraction peaks obviously increased. The average crystallite size of D was calculated from the FWHM of the diffraction peaks using the Debye–Scherrer equation (Klong and Alexander 1954). The size of the particles was not changed by the concentration of the dopants. The average crystallite sizes of ZnS and ZnS:Ni $^{2+}$ (1 %) were calculated as 4 and 4.5 nm, respectively. Moreover, the calculated sizes of the PMMA, PVP, PEG and CTAB capped ZnS:Ni $^{2+}$ nanoparticles are around 3.4, 3.7, 3.8 and 3.9 nm, respectively. By comparing the uncapped and capped particles, the capped particle sizes were significantly reduced due to prevention of the aggregation by coating the organic molecules on ZnS:Ni $^{2+}$. Among the various surfactants used, the PMMA capped ZnS:Ni $^{2+}$

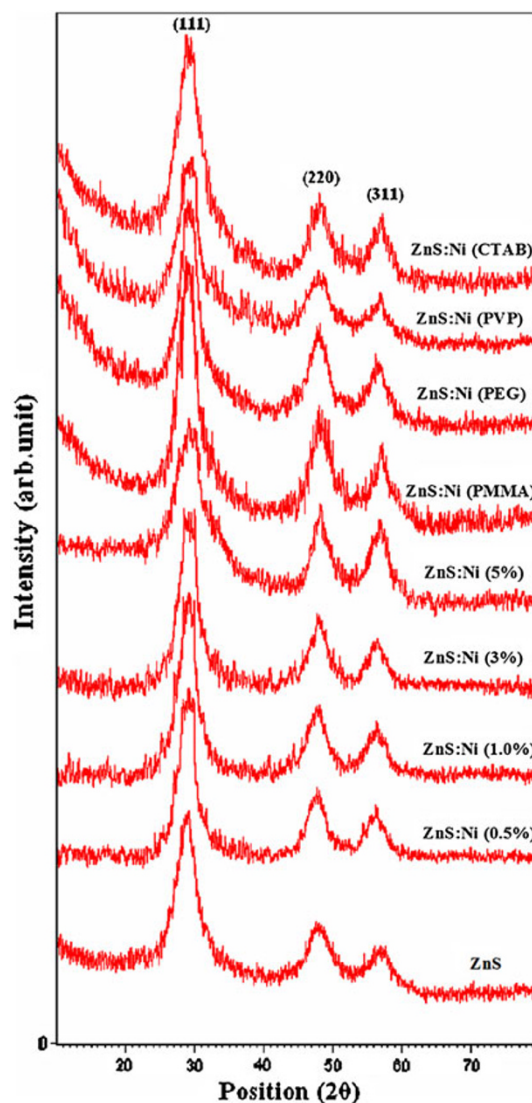


Fig. 1 X-ray diffraction patterns of ZnS, ZnS:Ni $^{2+}$ (0.5–5 %) and surfactant capped ZnS:Ni $^{2+}$ (1 %) nanoparticles

nanoparticles have smaller size than the others. It may be due the higher molecular weight (MW=1,20,000) of the PMMA. Generally, the total amount of the adsorbed polymer on growth particles is higher for higher molecular

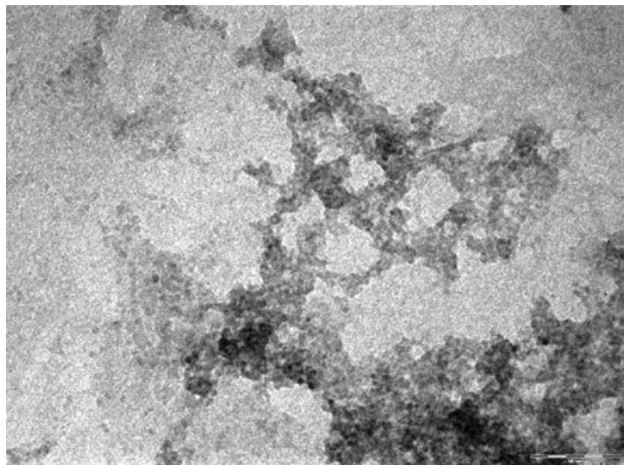


Fig. 2 TEM micrograph of uncapped ZnS:Ni²⁺ (1%) nanoparticles and corresponding SAED pattern (*inset*). The *scale bar* represents 50 nm

weight. When a large amount of polymer was adsorbed by the particles, stability of particles increases. Finally, the particles were isolated (Liufu et al. 2004).

Figures 2 and 3 show the TEM images of uncapped and various surfactant capped ZnS:Ni²⁺ nanoparticles. Figure 2 shows the TEM micrograph of ZnS:Ni²⁺ nanoparticles. As shown in figure, the particles are highly aggregated due to high surface energy of the growth particles in nanoscale. The average size of the individual particles from the TEM images is around 4.5 nm. The corresponding selected area electron diffraction (SAED) pattern (*inset*) of the sample is shown in Fig. 2. The diffraction rings for the samples indexed to the (1 1 1), (2 2 0) and (3 1 1) planes confirmed the cubic phase. Figure 3a–d shows TEM images of PMMA, PVP, PEG and CTAB capped ZnS:Ni²⁺ nanoparticles, respectively. The TEM images show that the synthesized particles are uniformly distributed. As could be seen, the single particle size was consistent with XRD results. The surface modified ZnS:Ni²⁺ nanoparticles show spherical with homogeneous size distribution. But the uncapped nanoparticles show as irregular shape. This may be due to the uncontrolled growth in the absence of the capping agent. From the TEM

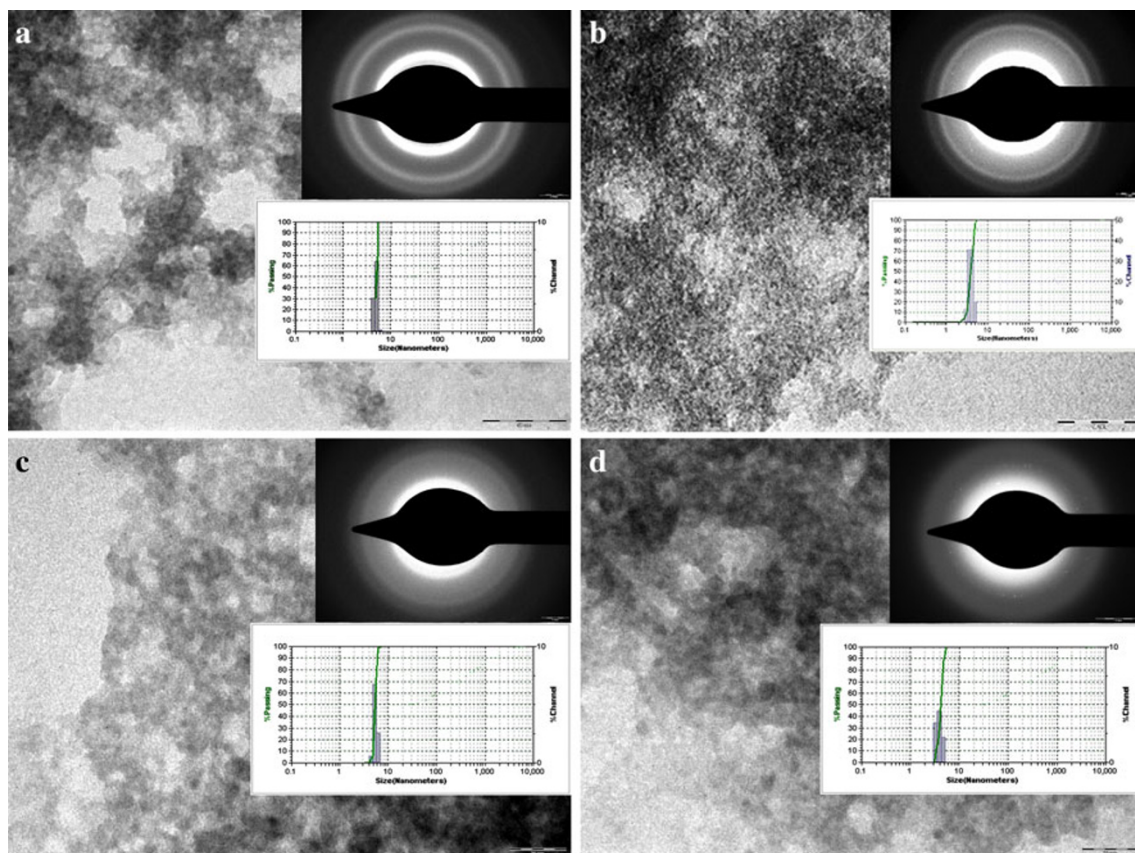


Fig. 3 TEM micrographs of surfactant (PMMA, PVP, PEG and CTAB) capped ZnS:Ni²⁺ (1%) nanoparticles and corresponding SAED pattern with particle size analyzer curve (*inset*). The *scale bars*

represented 100 and 50 nm for PMMA and PVP capped particles and 20 nm for PEG and CTAB capped ZnS:Ni²⁺ nanoparticles

micrographs, we could find that the surfactants played an important role in controlling the size and monodisperse of the ZnS:Ni²⁺ nanoparticles. Notably, the ZnS:Ni²⁺ nanoparticles that were passivated with PMMA has a small size and narrow size distribution compared with those other capping agents. The corresponding SAED patterns of the samples are shown in figures (inset). The three bright rings shows formation of cubic phase of ZnS:Ni²⁺ nanoparticles. In addition, the broaden fringes indicate the formation of very small particles. Moreover, the particle size analyzer curve (inset) of the PMMA (Fig. 3a), PVP (Fig. 3b), PEG (Fig. 3c) and CTAB (Fig. 3d) capped samples shows that the synthesized particles are highly monodispersed and small in size. These results are in good agreement with the corresponding XRD data mentioned above. The obtained XRD and TEM results indicate that the surfactant capped particles were in small size and homogeneous distribution. This means that the rapidly formed ZnS:Ni²⁺ clusters were immediately surrounded by the surfactants. As a result the particles were isolated.

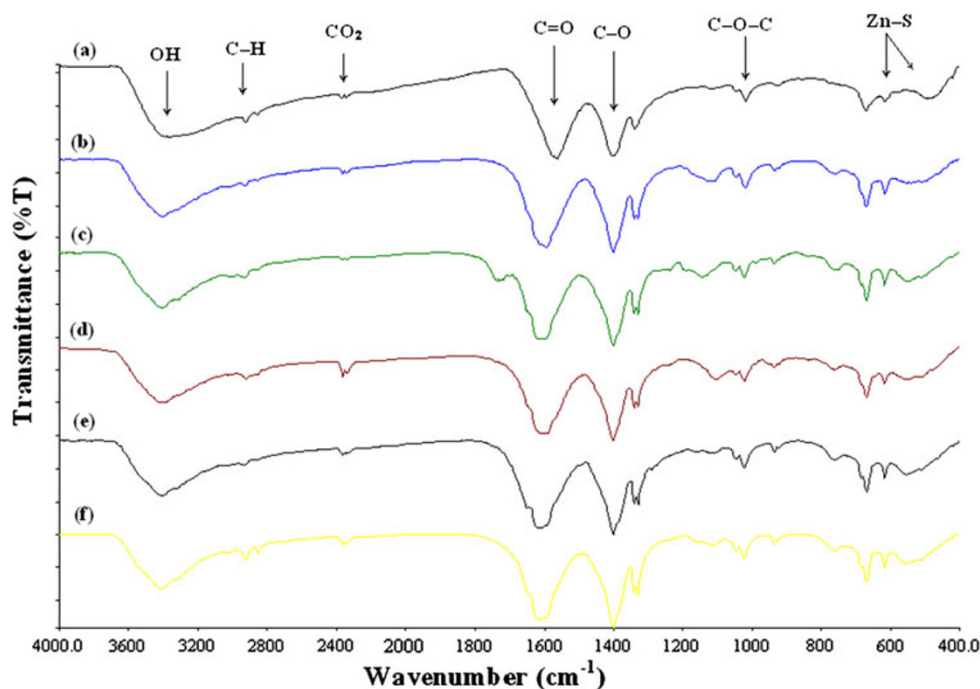
FT-IR study

FT-IR spectroscopy gives qualitative information about the way in which the adsorbed surfactant molecules are bound to the surface of ZnS:Ni²⁺ nanoparticles. FT-IR spectra of the undoped, Ni-doped ZnS and surfactant capped ZnS:Ni²⁺ nanoparticles were recorded in the range 4,000–400 cm⁻¹ and are shown in Fig. 4. The FT-IR analysis of the undoped ZnS and ZnS:Ni²⁺ nanoparticles show that the peaks appearing at 1,110, 618 and 491 cm⁻¹ are due to

Zn–S vibration and the peaks at 2,924, 2364 and 1,635 cm⁻¹ are due to microstructure formation of the samples. The obtained peak values are in good agreement with the reported values (Murugadoss 2010). The peak observed at 1,540 cm⁻¹ (C=O) in ZnS (Fig. 4a) curve is shifted to 1,600 cm⁻¹ when the dopant is included (Fig. 4b). It may be due to the presence of doping (Ni) ion in ZnS lattice site. Moreover, the peak at 1,400 cm⁻¹ of ZnS is split into two peaks at 1,331 and 1,341 cm⁻¹ for ZnS:Ni²⁺. In the spectrum of composite (Fig. 4c), the absorption bands at 1,700–1,750 cm⁻¹ are the characteristics of C=O stretching vibration of PMMA. In addition, the absorption bands at 1,150, 1,191, 1,240 and 1,269 cm⁻¹ are also representing C–O–C stretching vibration of PMMA (Kawaguchi 2001).

The peak observed at 1,636 indicates nitrogen–oxygen interaction of PVP (Fig. 4d). Furthermore, the intensity of the IR peaks for PVP capped particles (Fig. 4d) is higher than that of the uncapped ZnS:Ni²⁺ nanoparticles, which indicates the homogeneous formation of particles. The peaks at 1,512, 1,332 and 1,340 cm⁻¹ in Fig. 4e represent the formation of PEG on the surface of the ZnS:Ni²⁺ nanoparticles (Silverstein et al. 1981). The strong band of hydroxyl group in Fig. 4e shifted towards lower wavenumber side with the decrease in absorption from Fig. 4a indicates hydrogen bond formed in the ZnS:Ni²⁺/PEG interface (Santhiya et al. 1999). The spectrum of CTAB is presented in Fig. 4f. The strong peaks observed at 1,610 and 1,402 cm⁻¹ are shifted to long wavenumber side from the uncapped particles (Fig. 4a), indicating the presence of CTAB on the ZnS:Ni²⁺ surface. The broad peaks for all the samples (Fig. 4a–e) in the range of

Fig. 4 FT-IR spectra of **a** ZnS, **b** ZnS:Ni²⁺ (1 %), **c** ZnS:Ni²⁺/PMMA, **d** ZnS:Ni²⁺/PVP, **e** ZnS:Ni²⁺/PEG and **f** ZnS:Ni²⁺/CTAB nanoparticles



3,410–3,465 cm^{-1} correspond to –OH group. The presence of this band can be clearly attributed to the adsorption of same atmosphere water during FT-IR measurements. The bands at 1,500–1,650 cm^{-1} and at 2,370 cm^{-1} are due to the C=O stretching mode arising from the absorption of atmospheric CO_2 on the surface of the nanoparticles (Qadri et al. 1999).

Optical absorption

Absorption and fluorescence spectroscopy are powerful non-destructive techniques to explore the optical properties of semiconducting nanoparticles. The optical absorption of the undoped and different concentrations of Ni-doped ZnS nanoparticles have been analyzed in de-ionized water as shown in Fig. 5. Figure 6 shows an absorption spectra of ZnS:Ni^{2+} nanoparticles capped with PMMA, PVP, PEG and CTAB as capping agents. The absorption wavelengths are in the UV range for all the samples. A blank solution of de-ionized water and/or respective surfactant was taken as reference. All absorption curves exhibit an intensive absorption in the 280–320 nm range, owing to the relative large excitation binding energy. It is clearly shown in Fig. 5 that the absorption edges are approximately same for all the doped samples and do not show any shift by doping concentrations. This may be due to effective small percentage of dopants. Moreover, the narrow and symmetric absorption peaks are due to the homogeneous size distribution of the particles as reflected in TEM results. The absorption for bulk ZnS is 345 nm (Murugadoss 2010). Figure 5 shows absorption peak of undoped ZnS centered around 300 nm and ZnS:Ni^{2+} (0.5–5 %) centered at 312 nm. From the absorption spectra, the optimum concentration (1 %) of the doping ions (Ni^{2+}) was selected by the strong absorption. A significant blue shift was observed for surfactant capped (Fig. 6) nanoparticles compared to that of the bulk, undoped and Ni-doped ZnS nanoparticles. This blue shifting in excitonic absorption peak is attributed to the quantum size effect (Becker and Bard 1983). In the quantum confinement range, the band gap of the particles increases when particle size decreased, which resulted in the shift of the absorption peak towards the lower wavelength side. The band gap energy of the nanoparticles was calculated from a simple energy wave equation ($E = hc/\lambda$). The determined band gap energy for ZnS is 4.14 eV and the Ni (1 %)-doped ZnS is 4.03 eV. In addition, the determined band gap values for PMMA, PVP, PEG and CTAB capped particles are 4.33, 4.22, 4.21 and 4.19 eV, respectively. This shows that the PMMA is an effective capping agent for reduction of the particle size than the others. It may be due to the high molecular weight of PMMA (it is discussed briefly in “Crystal structure and

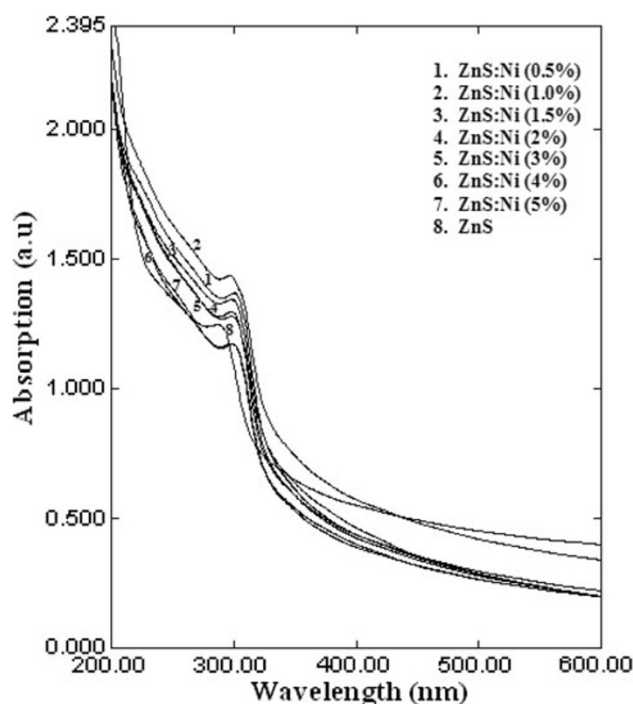


Fig. 5 UV–visible absorption spectra of ZnS and different concentrations of Ni (0.5–5 %)-doped ZnS nanoparticles

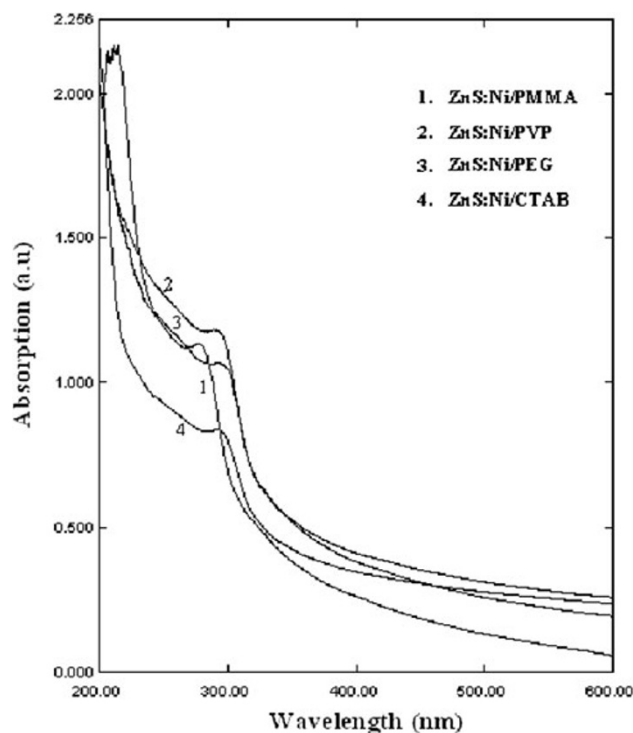


Fig. 6 UV–visible absorption spectra of different surfactant capped ZnS:Ni^{2+} (1 %) nanoparticles

Morphology”). This absorption spectrum has been used to calculate an approximate size for these nanoparticles using the Brus equation (Brus 1983, 1984).

$$E_{\text{gn}} = [E_{\text{gb}}^2 + 2h^2 E_{\text{gb}} (\pi/R)^2 / m^*]^{1/2} \quad (1)$$

where R is the radius of the size particles, E_{gn} and E_{gb} are the band gaps of nano and bulk systems, respectively, and m^* is the effective electron mass ($m^* = 0.22 m_e$). Based on the peak position in the absorption spectra, the size of these nanoparticles has been calculated as 3.72 nm for undoped and 4.46 nm for Ni^{2+} -doped ZnS. The surfactant capped ZnS:Ni^{2+} sizes were also calculated using the Brus equation as 3.40, 3.72, 3.75 and 3.9 nm for PMMA, PVP, PEG and CTAB capped ZnS:Ni^{2+} nanoparticles, respectively. It is in good agreement with XRD and TEM results. These particle sizes are comparable to the Bohr exciton radius of the bulk ZnS i.e., 2.5 nm (Qadri et al. 1999) (When the particle size is smaller than exciton Bohr radius, a large percentage of the atoms are on the particle surface, thus modifying the optical properties of the particle.)

Photoluminescence

A study of the photoluminescence (PL) property of any material is interesting because it can provide valuable information on the quality and purity of the material. The semiconductor nanoparticles, with sizes comparable to or below their exciton Bohr radius, have distinctive electronic and optical behaviors. These semiconductor nanoparticles absorb the light at specific wavelength and emit at longer wavelengths. Generally, emissions from semiconducting nanoparticles originate from electrons in the conduction band, excitonic states, and trap states. It is well known that emission and efficiency are very sensitive to nature of nanoparticles surface, due to the presence of gap surface states arising from surface non-stoichiometry and unsaturated bonds. Surface trap states allow non-radiative recombination and enhance luminescence efficiency. Broad low energy PL spectrum is usually attributed to trap state emissions arising from surface defect sites. Therefore, recording of PL spectrum is of paramount importance for estimating the size of nanoparticles and their characteristics for various applications. The room temperature photoluminescence (PL) spectra of undoped and different concentrations (0.5–5 %) of Ni^{2+} -doped ZnS nanoparticles were recorded in the visible region and are depicted in Fig. 7. It shows that the emission peak from undoped ZnS nanoparticles is appeared as symmetric and broadened around 445 nm, which could be ascribed from donor–acceptor pair. Different groups (Xiao and Xiao 2008; Qu et al. 2002; Yang et al. 2003) have studied the origin of the blue emission from undoped ZnS nanoparticle synthesized through chemical method. Chen et al. (2005) reported that the PL emission of ZnS nanoparticles is at 445 nm from donor–acceptor pair. The average size of the ZnS was 3 nm. Xiao and Xiao (2008) reported that the PL emission

of the ZnS nanoparticles is at 460 nm, which could be assigned to the radiative recombination involving effect states in the ZnS. They prepared particle size around 2 nm.

The PL position of the ZnS was tuned by adding impurity (Ni) as shown in Fig. 7. All the PL spectra of Ni^{2+} -doped ZnS nanoparticles are red shifted from the undoped ZnS. This implies that the dopant is created a trap state between the valance and conduction band. Hence, a least quantum of energy was provided to the nearest neighbor atom or lattice when the electron transition from the conduction band to trap state. As a result, the emission energy is reduced. It is worth noting that with the increase of the doping concentration, the peak position of this emission band shifts from blue to green region. Qu et al. observed the similar red shift for ZnS:Eu nanoparticles with increasing doping levels (Qu et al. 2002). In addition, relative intensity of the Ni-doped ZnS nanoparticles was reduced by increase in the Ni concentrations. The PL quenching is may be due to increase in the radiationless transition by the higher concentration of the nickel ions.

Yang et al. (2003) reported the PL emission of the Ni-doped ZnS nanoparticles (a single peak at 520 nm) using NiSO_4 as a source for Ni ions. But in this work, two new peaks were observed (instead of a single peak) using $\text{Ni}(\text{CH}_3\text{COO})_2$ as a source for Ni ions. In ZnS: Ni^{2+} semiconductor nanomaterials, the lowest multiplet term ^3F of the free Ni^{2+} ion is split into $^3\text{T}_1$, $^3\text{T}_2$ and $^3\text{A}_2$ through the anisotropic hybridization. Due to the d–d optical transitions of Ni^{2+} , the luminescent center of Ni^{2+} is formed in ZnS (Yang et al. 2002). Thus, the blue and green luminescences have been observed from Ni^{2+} -doped samples. As seen in Fig. 7, for all Ni-doped samples two emission peaks were observed, one is the blue region at 472 nm and another one is green emission at 498 nm arising from the recombination between the shallow donor level (sulfur vacancy) and

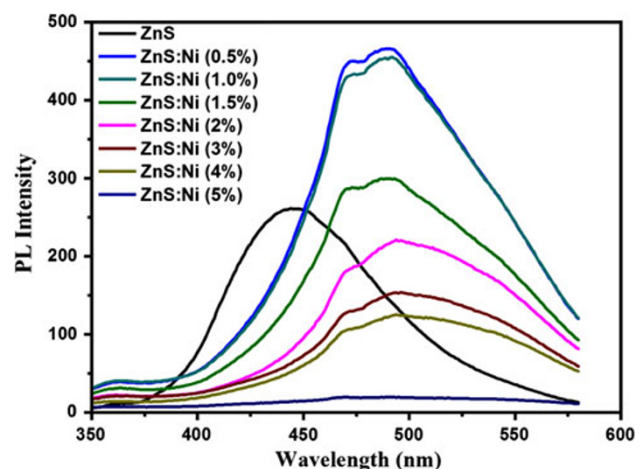


Fig. 7 PL spectra of different concentration of Ni (0.5–5 %) -doped ZnS nanoparticles

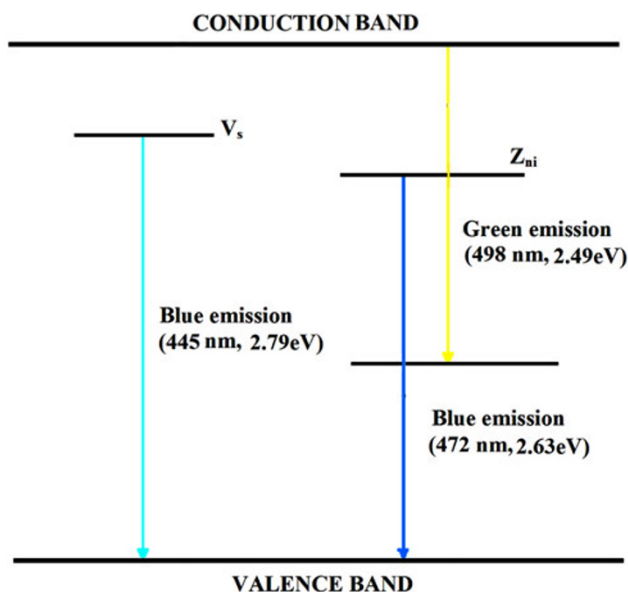


Fig. 8 Energy level diagram of undoped and Ni-doped ZnS

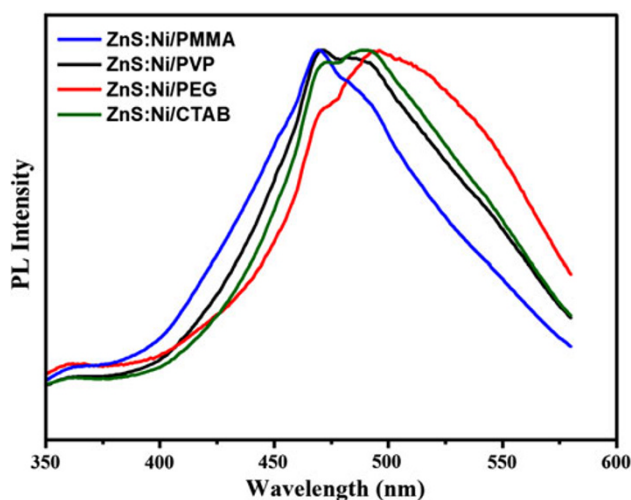


Fig. 9 PL spectra of different surfactant capped ZnS:Ni²⁺ (1%) nanoparticles

the ${}^3T_2-{}^3A_2$ transition of Ni²⁺ ions, respectively. Based on the PL results observed, the schematic energy-level diagram of ZnS:Ni²⁺ nanoparticle is depicted as shown in Fig. 8. Here V_s stands for sulfur vacancy and Z_{ni} stands for interstitial zinc. This figure explains the emission mechanism of ZnS:Ni²⁺ nanoparticles and illustrates the above assignment.

Figure 9 shows PL emission of different surfactant (PMMA, PVP, PEG and CTAB) capped ZnS:Ni²⁺ (1%) nanoparticles. The peak position of surfactant capped particles is similar to the uncapped ZnS:Ni²⁺. But the peak position is slightly varied. This may be due to the reduction particle size with respect to capping agent. In addition, the

band width of the PL emission is narrower than the uncapped ZnS:Ni²⁺. It indicates narrow size distribution. Moreover, the enhancement of the PL intensity indicates the increasing of crystallinity and reduction of the surface defect. By comparing the PL emissions, the intensity of PMMA capped particles is significantly blue shifted than the other capped particles. It dictates, the PMMA is an excellent particle size controller. The PL emissions are slightly red shifted capped with PVP, PEG and CTAB particles. It show increasing the particles or limiting the size control. However, the surfactants are acting a vital role to growth homogeneous particles.

Conclusions

ZnS:Ni²⁺ nanoparticles with very narrow size distribution were prepared from chemical precipitation method in aqueous medium at air atmosphere. The TEM images of all the surfactant capped ZnS:Ni²⁺ nanoparticles show that the particles are almost spherical in shape with homogeneous distribution.

ZnS:Ni²⁺ nanoparticles were successfully capped and the surface is modified by bio-compatible organic materials (PMMA, PVP, PEG and CTAB). Among the different capping agents, PMMA is more effective than others. The capped ZnS:Ni²⁺ nanoparticles show better dispersion as they were adsorbed on the surface of nanoparticles so as to fulfill the steric hindrance between nanoparticles and prevent agglomeration. Successful surface modification and bio-organic interface make the ZnS:Ni²⁺ nanoparticles suitable for use in nanoscale fluorescent probes for biological and medicinal applications such as targeted drug delivery, ultra-sensitive disease detection and labeling of biological cells. UV light is absorbed effectively by ZnS:Ni²⁺ nanoparticles, so that they can be used in sunscreens.

Acknowledgments The author would like to acknowledge the service rendered by scientific officers of IIT Bombay, Mumbai, CECRI, Karaikudi, STIC, Cochin and CISL, Annamalai University, for recording TEM, XRD, and FT-IR spectra. The author also likes to thank Dr. N. Rajendran, Department of Chemistry, Annamalai University, India, for providing UV-visible and PL facility.

Open Access This article is distributed under the terms of the Creative Commons Attribution License which permits any use, distribution, and reproduction in any medium, provided the original author(s) and the source are credited.

References

- Alivisatos AP (1996) Semiconductor clusters, nanocrystals, and quantum dots. *Science* 271:933–937
- Becker WG, Bard AJ (1983) Photoluminescence and photoinduced oxygen adsorption of colloidal zinc sulfide dispersions. *J Phys Chem* 87:4888–4893

- Brus LE (1983) A simple model for the ionization potential, electron affinity, and aqueous redox potentials of small semiconductor crystallites. *J Chem Phys* 79:5566–5571
- Brus LE (1984) Electron–electron and electron-hole interactions in small semiconductor crystallites: the size dependence of the lowest excited electronic state. *J Chem Phys* 80:4403–4409
- Brus L (1986) Electronic wave functions in semiconductor clusters: experiment and theory. *J Phys Chem* 90:2555–2560
- Brus L (1991) Quantum crystallites and nonlinear optics. *Appl Phys A* 53:465–474
- Chen W, Aguekian VF, Vassiliev N, Serov AY, Filosofov NG (2005) New observations on the luminescence decay lifetime of Mn^{2+} in $ZnS:Mn^{2+}$ nanoparticles. *J Chem Phys* 123:124707
- Counio G, Esnouf S, Gacoin T, Boilot JP (1996) $CdS:Mn$ nanocrystals in transparent xerogel matrices: synthesis and luminescence properties. *J Phys Chem* 100:20021–20026
- Devisschere P, Neyts K, Corlatan D, Vandenbossche J, Barthou C, Benalloul P, Benoit J (1995) Analysis of the luminescent decay of $ZnS:Mn$ electroluminescent thin films. *J Lumin* 65:211–219
- Fang YC, Chu SY, Chen HC, Kao PC, Chen IG, Hwang CS (2009) Effect of the S/Zn ratio on the photoluminescence properties of color-tunable $ZnS:Mn$ nanophosphors. *J Electrochem Soc* 156:K55–K58
- Feltin N, Levy L, Ingert D, Pileni MP (1999) Magnetic properties of 4 nm $Cd_{1-x}Mn_xS$ nanoparticles differing by their compositions, y . *J Phys Chem B* 103:4–10
- Green AA, Hersam MC (2008) Colored semitransparent conductive coatings consisting of monodisperse metallic single-walled carbon nanotubes. *Nano Lett* 8:1417–1422
- Hoffman AJ, Mills G, Yee H, Hoffmann MR (1992) Q-sized cadmium sulfide: synthesis, characterization, and efficiency of photoinitiation of polymerization of several vinylic monomers. *J Phys Chem* 96:5546–5552
- Huang CM, Chen LC, Pan GT, Yang TCK, Chang WS, Cheng KW (2009) Effect of Ni on the growth and photoelectrochemical properties of ZnS thin films. *Mater Chem Phys* 117:156–162
- Igarashi T, Isobe T, Senna M (1997) EPR study of Mn^{2+} electronic states for the nanosized $ZnS:Mn$ powder modified by acrylic acid. *Phys Rev B* 56:6444–6445
- Kar S, Biswas S (2008) White light emission from surface-oxidized manganese-doped ZnS nanorods. *J Phys Chem C* 112:11144–11149
- Kawaguchi H (2001) Functional polymer microspheres. *Prog Polym Sci* 25:1171–1210
- Kennedy TA, Glaser ER, Klein PB, Bhargava RN (1995) Symmetry and electronic structure of the Mn impurity in ZnS nanocrystals. *Phys Rev B* 52:14356–14359
- Klimov VI, Ivanov SA, Nanda J, Achermann M, Bezel I, McGuire JA, Piryatinski A (2007) Single-exciton optical gain in semiconductor nanocrystals. *Nature* 447:441–446
- Klong HP, Alexander LF (1954) X-ray diffraction procedures for crystalline and amorphous materials. Wiley, New York
- Liufu S, Xiao H, Li Y (2004) Investigation of PEG adsorption on the surface of zinc oxide nanoparticles. *Powder Technol* 145:20–24
- Murugadoss G (2010) Synthesis and optical characterization of PVP and SHMP-encapsulated Mn^{2+} -doped ZnS nanocrystals. *J Lumin* 130:2207–2214
- Murugadoss G, Rajamannan B, Ramasamy V (2010) Synthesis, characterization and optical properties of water-soluble $ZnS:Mn^{2+}$ nanoparticles. *J Lumin* 130:2032–2039
- Ong HC, Chang RPH (2001) Optical constants of wurtzite ZnS thin films determined by spectroscopic ellipsometry. *Appl Phys Lett* 79:3612–3614
- Pohl UW, Gumlich HE (1989) Optical transitions of different Mn-ion pairs in ZnS. *Phys Rev B* 40:1194–1201
- Qadri SB, Skelton EF, Hsu D, Dinsmore AD, Yang J, Gray HF, Ratna BR (1999) Size-induced transition-temperature reduction in nanoparticles of ZnS. *Phys Rev B* 60:9191–9193
- Qu SC, Zhou WH, Liu FQ, Chen NF, Wang ZG, Pan HY, Yu DP (2002) Photoluminescence properties of Eu^{3+} -doped ZnS nanocrystals prepared in a water/methanol solution. *Appl Phys Lett* 80:3605–3607
- Sampra S, Sarma DD (2004) Evolution of the electronic structure with size in II–VI semiconductor nanocrystals. *Phys Rev B* 69:125304
- Santhiya D, Subramanian S, Natarajan KA (1999) Surface chemical studies on the competitive adsorption of poly(acrylic acid) and poly(vinyl alcohol) onto alumina. *J Colloid Interface Sci* 216:143–153
- Silverstein RM, Bassler GC, Morrill TC (1981) Spectrometric identification of organic compounds, 4th edn. Wiley, New York
- Toyama T, Hama T, Adachi D (2009) An electroluminescence device for printable electronics using coprecipitated $ZnS:Mn$ nanocrystal ink. *Nanotechnology* 20:055203
- Wang Z, Daemen LL, Zhao Y, Zha CS, Downs RT, Wang X, Wang ZL, Hemley RJ (2005) Morphology-tuned wurtzite-type ZnS nanobelts. *Nat Mater* 4:922–927
- Xiao Q, Xiao C (2008) Synthesis and photoluminescence of water-soluble Mn^{2+} -doped ZnS quantum dots. *Appl Surf Sci* 254:6432–6435
- Yang P, Lu MK, Xu D, Yuan D, Chang J, Zhou GJ, Pan M (2002) Strong green luminescence of Ni^{2+} -doped ZnS nanocrystals. *Appl Phys A Mater Sci Process* 74:257–259
- Yang P, Lu M, Xu D, Yuan D, Song C, Liu S, Cheng X (2003) Luminescence characteristics of ZnS nanoparticles co-doped with Ni^{2+} and Mn^{2+} . *Opt Mater* 24:497–502
- Yu JQ, Liu HM, Wang YY, Jia WY (1998) Hot luminescence of Mn^{2+} in ZnS nanocrystals. *J Lumin* 79:191–199